Hydrology and Earth System Sciences Discussions

European summer climate modulated by NAO-related precipitation

G. Wang[1], **A. J. Dolman**[1], **and A. Alessandri**[2]

[1]Department of Hydrology and Geo-environmental Sciences, Faculty of Earth and Life Sciences, VU University Amsterdam, De Boelelaan 1085, 1081 HV Amsterdam, The Netherlands
[2]Centro Euro-Mediterraneo per i Cambiamenti Climatici, Via Aldo Moro 44, 40127 Bologna, Italy

Correspondence to: G. Wang (gwang.vu@gmail.com)

Title Page

Abstract	Introduction
Conclusions	References
Tables	Figures

◀◀   ▶▶

◀   ▶

Back   Close

Full Screen / Esc

Printer-friendly Version

Interactive Discussion

Title Page

Abstract | Introduction

Conclusions | References

Tables | Figures

◀◀ | ▶▶

◀ | ▶

Back | Close

Full Screen / Esc

Printer-friendly Version

Interactive Discussion

Abstract

Recent summer heat waves in Europe were preceded by precipitation deficits in winter. Numerical studies suggest that these phenomena are dynamically linked by land-atmosphere interactions. However, there is still no clear evidence that connects summer climate variability to winter precipitation and the relevant circulation pattern so far. Using a technique specially designed for detecting directional influences between climatic fields, we investigate the statistical responses of summer mean as well as maximum temperature variability (June–August, T_{mean} and T_{max}) to preceding winter precipitation (January–March, P_{JFM}) for the period 1901–2005. There appear distinctive T_{mean} and T_{max} responses to P_{JFM} over the Mediterranean, where it is most sensitive to land-atmosphere interactions. An analysis of soil moisture proxy (self-calibrating Palmer drought severity index, scPDSI) shows that the P_{JFM} seems to influence summer temperature via soil moisture, and therefore the T_{mean} and T_{max} responses we present here are very likely to be physical hints of water cycle interactions with temperature. We estimate that roughly 10~20% of the interannual variability of T_{max} and T_{mean} over the Mediterranean is forced by P_{JFM}; for the scPDSI, these values amount to 20~25%. Further analysis shows that these responses are highly correlated to the North Atlantic Oscillation (NAO) regime over the Mediterranean. Therefore we suggest that NAO modulates European summer temperature via controlling precipitation that initializes the moisture states of water cycle interactions with temperature. This clear picture of relations between European summer climate and NAO-related precipitation suggests potential for improved seasonal prediction of summer climate in particular extreme events.

1 Introduction

The recent European climate is characterized by an increasing frequency of summer heat waves with substantial societal and ecological impacts, e.g. the record-breaking heat wave in 2003. Climate projections point towards even higher-frequent

and longer-lasting heat waves under increased greenhouse gas emission scenarios (Scherrer et al., 2005; Pal et al., 2004; Stott et al., 2004; Meehl et al., 2004). These past and projected heat waves highlighted the importance of a detailed understanding of the mechanisms that contribute to the initialization and persistence of extreme heat
5 conditions. Hot and dry summers in Europe are generally associated with a specific, large-scale anticyclonic atmosphere circulation regime (Cassou et al., 2005; Fischer et al., 2007). Most of hot and dry summers over Europe were preceded by pronounced deficits of precipitation in winter and early spring (Della-Marta et al., 2007; Vautard et al., 2007). Vautard et al. (2007) showed with the mesoscale MM5 model that the
10 observed winter precipitation deficit and summer heat wave were dynamically linked via land-atmosphere feedback loops, wherein soil moisture played a crucial role. The deficit of precipitation and subsequent drier soils resulted in reduced latent cooling and thereby an increase of air temperature, in agreement with other numerical experiments (e.g., Seneviratne et al., 2006; Fischer et al., 2007; Zampieri et al., 2009).

15   These investigations of individual heat waves highlighted the role of land-atmosphere interactions particularly between winter precipitation and subsequent soil moisture states but also pointed to the importance of circulation patterns in the generation of summer heat waves. An immediate question that arises is whether this land surface feedback mechanism exists only for extraordinary hot summers or more systematically.
20 Schär et al. (2004) underlined that an increase of interannual temperature variability in response to greenhouse-gas forcing might be an alternative causal mechanism for the occurrence of European summer heat waves; and numerical analysis with prescribed soil moisture by Seneviratne et al. (2006) suggested further that the increased interannual temperature variability is strongly related to the land-atmosphere interactions.

25   However, there exists as yet no clear analysis of observational evidence connecting summer temperature to interannual variability of winter precipitation. The present paper aims to fill this gap in our understanding by investigating with long-term observations the summer temperature variability, including mean and maximum, in relation to the interannual variability of winter precipitation and possible relevant circulation regimes.

European summer climate modulated by NAO-related precipitation

G. Wang et al.

Title Page

Abstract	Introduction
Conclusions	References
Tables	Figures

|◄| |►|

|◄| |►|

Back | Close

Full Screen / Esc

Printer-friendly Version

Interactive Discussion

Furthermore, we use a soil moisture proxy to clarify if these responses are related to soil moisture processes. The paper is organized as follows: in Sect. 2 the observational datasets used are described and the analysis technique is briefly introduced. Section 3 is dedicated to the results and, finally, Sect. 4 contains a discussion and the conclusions of this study.

2 Datasets and methods

2.1 Datasets

We use long-term gridded observations of accumulated precipitation in January–March (P_{JFM}) and averaged daily mean as well as maximum temperature in summer (June–August, T_{mean} and T_{max}, respectively) for the period 1901–2005, derived from University of East Anglia Climatic Research Unit (CRU) at a horizontal resolution of $0.5°×0.5°$ (Mitchell et al., 2005). The P_{JFM} values over mountain Scandinavia are not included in this study. Due to the sparseness of in situ soil moisture observations, the averaged self-calibrating Palmer drought severity index in June–August (scPDSI, Wells et al., 2004) is used as a proxy of soil moisture. The scPDSI is based on soil water content in a rather complex water budget model involving water cycle interactions with temperature; therefore it is suitable for the purpose of this study. Ideally one would use remotely sensed soil moisture observations (e.g., de Jeu et al., 2008) but the datasets are unfortunately not yet sufficiently long in time. The scPDSI dataset obtained from CRU spans 1901–2002 on a monthly basis and range from −4 to +4 in the case of extremely dry and extremely wet conditions, respectively (van der Schrier et al., 2006).

2.2 Coupled manifold technique

Widely used methods to detect coupling between climatic fields are variance analysis methods, such as Maximum Covariance Analysis (MCA, also termed as SVD) to

Title Page

Abstract | Introduction

Conclusions | References

Tables | Figures

◄ | ►

◄ | ►

Back | Close

Full Screen / Esc

Printer-friendly Version

Interactive Discussion

maximize explained covariance or canonical correlation analysis (CCA) to maximize correlations. These traditional methods require orthogonal solutions with little physical justification, and can detect unfortunately only cross-correlation between fields. However, the climate system is full of interactions and a cross-correlation provides little information of directional influences between fields. Recently, Navarra and Tribbia (2005) proposed a non-orthogonal solution for this problem, the Coupled Manifold Technique (CMT), which enables to detect the directional interactions. It is mathematically demonstrated that the CMT technique provides a framework that generalizes the traditional methods for variance analysis, such as SVD, CCA and regression analysis.

Assuming that the relation between two given fields Z and S is linear, the CMT looks for the response of Z to S using a linear operator A that satisfies

$$A = \min\|Z - AS\|^2, \tag{1}$$

where the norm is the Frobenius norm, defined by

$$\|Z\|^2 = \text{trace}(ZZ'), \tag{2}$$

and the primes denotes a matrix transpose operation. Using the Procrustes method (Richman et al., 1993), the A solution can be written as

$$A = ZS'(SS')^{-1}. \tag{3}$$

The operator A represents the influence of S on Z. Using A we can separate the field Z into two parts:

$$Z_{\text{for}} = AS,$$
$$Z_{\text{free}} = Z - AS. \tag{4}$$

The Z_{for} part is the portion of the field variability that is forced by the S variability (henceforth "forced manifold"), while Z_{free} is the portion independent from S ("free manifold").

In the same way, that part of S field forced by Z variability can be isolated by reversing the input-output roles of the two fields. Since the direction of influence between

Title Page

Abstract	Introduction
Conclusions	References
Tables	Figures

◄◄	►►
◄	►
Back	Close

Full Screen / Esc

fields is taken into account, the CMT technique detects causality rather than cross-correlation, and thus constitutes a significant improvement over traditional SVD and CCA techniques. The CMT has been used to study directional interactions between vegetation and atmosphere, showing good performance (Alessandri et al., 2008). To simplify the computation, this technique is applied to the EOF coefficients of fields of interest in our study, as suggested by Navarra and Tribbia (2005), with 99% of the total variance of each field retained. Furthermore, each element of A is tested against the null hypothesis of being equal to zero at the 1% significance level based on the Student t distribution as described by Cherchi et al. (2007). This method may identify both one-way and two-way relations between fields. In our analysis, there exist time lags between fields, and therefore we end up with only one-way relation, that is, only the variability in Z forced by S. When the forced manifold is obtained, a further significance test of the forced variance is performed to make the result robust using a Monte Carlo approach. Then S and the forced manifold Z_{for}, containing now only the variability in Z forced by S, are subjected to traditional MCA to obtain the forcing and forced patterns as well as time coefficient series of interest.

3 Results

3.1 Responses of T_{mean} and T_{max} to P_{JFM}

Figure 1a shows the percentage of T_{mean} variance forced by the P_{JFM} variability, and that for T_{max} is shown in Fig. 1d. These values are derived from the ratio of the forced T_{mean} (T_{max}) manifold to the original T_{mean} (T_{max}) fields. We tested where the percentage values are significant different from zero at the 0.10 level. For each grid point, we tested the null hypothesis of getting as high or higher variance fractions through a Monte Carlo bootstrap method (10 000 repetitions of the CMT) by randomizing the order number of P_{JFM} values on each grid. The largest values are found over Southern Europe for both T_{mean} and T_{max} where it is most sensitive to land-atmosphere interactions (Seneviratne

European summer climate modulated by NAO-related precipitation

G. Wang et al.

et al., 2006; Fischer et al., 2007; Zampieri et al., 2009), while little forcing (low values) is observed over Northern Europe of 50° N. Up to 5∼15% of the summer T_{mean} variance over Southern Europe appears to be forced by P_{JFM}. The forced T_{mean} variance by P_{JFM} is up to 8% over Western Europe, averaged within the green rectangle in Fig. 1a, which

5   doesn't pass the significance test. Over Eastern Europe, this value increases to 11% averaged within the red rectangle in Fig. 1a, passing the significance test. This implies that summer T_{mean} over Eastern Europe is more sensitive to P_{JFM}. These values for T_{max} are a bit higher. The forced T_{max} variance is up to 10% over Western Europe and that value over Eastern Europe is up to 14%, averaged within the green as well as the

10   red rectangles, respectively in Fig. 1d. Low values for both T_{mean} and T_{max} over North of 50° N indicate little influence from P_{JFM}.

The MCA analysis was originally designed for detecting cross-correlation. In our study it is conducted to the P_{JFM} field and the T_{mean} (T_{max}) manifold forced by the P_{JFM} variability, and therefore what it detects is the forcing P_{JFM} pattern and the T_{mean} (T_{max})

15   response. Derived from the first MCA mode, Fig. 1b and c shows the 1st pair of forcing P_{JFM} pattern and its T_{mean} response, containing 95% of the total squared covariance. This MCA mode exhibits unit correlated time coefficients ($r>0.999$), suggesting the derived forcing-forced relationship is very robust. The time coefficient series are shown as blue lines in Fig. 3. We note that the unit correlation derived here is due to the data

20   preprocessing with CMT, which constructs only the T_{mean} variability forced by P_{JFM} at significance level of 0.01. The time coefficient series of the 1st MCA mode without CMT exhibit a correlation of 0.40 (not shown), which is clearly insufficient to conclude a significant linkage. The same situation also holds in the following analysis of T_{max} as well as soil moisture proxy of scPDSI.

25   Shown in Fig. 1b and c, there exists only one significant P_{JFM} anomaly over the Mediterranean, with opposite sign of the T_{mean} response largely northward and eastward extended to 50° N compared to the P_{JFM} anomaly. This suggests that T_{mean} in summer fluctuates in correspondence to the anomalous states of P_{JFM} via the cooling effect of the surface energy balance. Precipitation is spectrally white with very limited

memory up to two weeks due to the chaotic nature of atmosphere (Wang et al., 2010); therefore the extended memory of P_{JFM} is probably sustained by soil moisture feedbacks on precipitation. One may question the existence of forced T_{mean} anomalies in the opposite sign over north of 50° N. It appears not a physical response to P_{JFM} since there exists no forcing anomaly in P_{JFM} in the very location. Therefore we attribute it to be a statistical coexistence with no physical implication. Furthermore, this anomaly accounts for a very low percentage of the forced T_{mean} variance over north of 50° N (Fig. 1a) and did not pass our significance test.

Shown in Fig. 1e and f is the 1st leading pair of the forcing P_{JFM} pattern and its T_{max} response, which contains 96% of the total squared covariance with unit correlated time coefficient series ($r > 0.999$, blue lines in Fig. 3). Comparing Fig. 1b and e, we can see clearly the T_{max} anomaly is forced by almost the same P_{JFM} anomaly as that forces T_{mean}. Furthermore, these time coefficient series are nearly unit correlated with those derived from the $P_{JFM} \sim T_{mean}$ association ($r > 0.999$). These statistical properties suggest that the derived linkages between P_{JFM} and T_{mean} as well as T_{max} are very likely to be driven by the same climate dynamics. The forced T_{max} (Fig. 1f) exhibits very similar dipole pattern as T_{mean} (Fig. 1c), however, the percentage of forced variance over north of 50° N is small again.

An important question regarding land-climate interactions is whether they lead to amplified variability of climate extremes, such as heat waves, particularly in the context of climate change (Seneviratne et al., 2010). Over south of 50° N, the percentage of T_{max} variance forced by P_{JFM} appears to be more homogenized than that of T_{mean}. Furthermore, the robust relations derived from MCA analysis after CMT enable us to compare the magnitudes of T_{mean} and T_{max} responses to P_{JFM}, where the magnitude of the T_{max} response appears to twice that of T_{mean}. Therefore P_{JFM} exerts to some extend larger influence on T_{max} than that on T_{mean} over south of 50° N, possibly through water cycle interactions.

3.2 The role of soil moisture

So far we have shown that summer temperature fluctuates in relation to fluctuations in winter precipitation over Mediterranean. It is plausible to hypothesize that these responses are modulated by interactions between the water cycle and temperature with soil moisture playing a critical mediating role. An analysis of soil moisture would help to support this hypothesis. For this purpose the same analytic framework as above is conducted to P_{JFM} and summer scPDSI as a soil moisture proxy. Analysis of this field is expected to clarify the role of soil moisture in the forced T_{max} and T_{mean} responses to P_{JFM}. This analysis is restricted to south of 55° N where P_{JFM} has distinctive expressions in the T_{max} and T_{mean} fields.

The scPDSI variability forced by P_{JFM} is shown in Fig. 2. Shaded values in Fig. 2a indicate the percentage of scPDSI variance forced by P_{JFM} that can pass significance test at 0.01 level, with the largest values of 20~25% existing in the West Mediterranean. The 1st MCA mode contains 80% of the total square covariance with unit correlated time coefficient series ($r>0.999$, green lines in Fig. 3). The forcing P_{JFM} pattern exhibits a distinctive anomaly over Mediterranean (Fig. 2b), very similar to that P_{JFM} patterns forcing T_{mean} and T_{max} (Fig. 1a, d). The scPDSI response is of the same sign but largely northward and eastward extended (Fig. 2c) compared to the forcing P_{JFM} pattern. Of particular interest is that the time coefficient series are highly correlated with those from temperature analyses in Sect. 3.1, with correlation coefficient $r>0.999$. The MCA analyses are summarized in Table 1. Therefore the responses of scPDSI, T_{mean} and T_{max} to the P_{JFM} variability we present here appear to be driven by the same climate dynamics, and P_{JFM} is very likely to influence T_{mean} and T_{max} via soil moisture. That is, a negative precipitation anomaly in winter is supposed to result in summer heating due to reduced latent cooling from soil moisture. The reverse relationship also holds, where a positive precipitation anomaly implies cooling.

These observational relations corroborate the interactions between water cycle and temperature established in previous numerical work, e.g., Seneviratne et al. (2006).

Note that if we perform the same set of statistics to the winter precipitation and summer minimum temperature, we do not obtain the same relations. This is physically reasonable because the minimum temperature is highly constrained by external forcings, such as atmospheric circulation and sea surface temperature, rather than internal feedbacks (Alfaro et al., 2006; Zhang et al., 2008).

3.3 Link to North Atlantic Oscillation

The North Atlantic Oscillation (NAO) is the dominating large-scale atmospheric circulation over the Atlantic-Europe sector in winter, with marked influence on winter climate. In recent years, the NAO is also observed to influence summer climate over Europe, in a weak but significant way. For example, Qian et al. (2003) showed with observations that European summer temperature has positive correlation with the NAO index in previous January and February; Kettlewell et al. (2003) discovered a negative correlation between winter NAO and summer precipitation over Europe. However, the mechanism that links these phenomena remains still a puzzle. The derived forcing P_{JFM} patterns on T_{mean} and T_{max} as well as scPDSI in our analysis appear to resemble the NAO regime over Mediterranean, suggesting a plausible hypothesis that the NAO variability modulates summer climate over Europe through controlling winter precipitation that subsequently initializes the moisture states of water cycle interactions with temperature.

To further clarify the role of NAO in these processes, we compared the winter NAO index and the time coefficient series derived from MCA analysis. We use the averaged values of NAO index in January–March for the period 1901–2005, based on the difference of normalized sea level pressures between Gibraltar, the Azores and SW Iceland. Shown in Fig. 3, the derived time coefficient series from T_{mean}, T_{max} and scPDSI analyses have a high correlation with the NAO index with $r=0.65$ ($p<0.05$), suggesting a significant relation between the NAO variability and summer climate. The NAO variability is a north-south shift (or vice versa) in the track of storms and depressions across the North Atlantic Ocean and into Europe. The Atlantic storms that travel

into Europe result in a dry Mediterranean Europe during a high NAO winter and the opposite during a low NAO winter (Hurrell et al., 2001). Based on the above analysis, we suggest that the NAO regime over the Mediterranean modulates European summer climate via initialization of the winter land surface moisture.

4   Discussion and conclusion

The importance of soil moisture initialization in winter and early spring for the seasonal prediction of heat and drought waves in European summer has been demonstrated in recent years (e.g., Vautard et al., 2007; Fischer et al., 2007; Zampieri et al., 2009; Seneviratne et al., 2006; Ferranti et al., 2006). Although soil moisture is closely related to precipitation, a clear picture of the relations between summer climate and preceding winter precipitation has not yet been demonstrated observationally. This is largely because the expected signal is very weak in the fields of interest, and traditional techniques for cross-correlation, such as MCA and CCA, are not capable of generating robust relations from this strong background noise.

Using the newly developed CMT technique that detects directional influence between climatic fields, we present in this paper robust responses of summer T_{mean} and T_{max} as well as scPDSI to previous winter precipitation. Distinctive responses exist only over the Mediterranean area, where the temperature response is most sensitive to land-atmosphere interactions in regional climate models (Schär et al., 1999; Seneviratne et al., 2006). The P_{JFM} variability accounts for up to 10~15% of the total T_{mean} and T_{max} variance, respectively for the period of 1901–2005; for the scPDSI this value amounts to 20~25% over the Western Mediterranean. The P_{JFM} appears to influence T_{mean} and T_{max} via scPDSI, agreeing very well with our recent understanding of the water cycle dynamics over land (see Seneviratne et al., 2010 for a review). Therefore our findings are very likely to be physical of origin, although there is always a risk to infer physics from statistics. We also note that we are not addressing the full picture of land-atmosphere feedback processes but only that part that is related to January–March precipitation.

The extension of responses towards north and east is also observed in numerical experiments. Vautard et al. (2007) suggested that the northward propagation may be due to the southerly wind episodes carrying moisture northward. The eastward propagation is probably due to the heat low response over Central Europe, blocking the

5 inflow of moist maritime air from the Atlantic and reinforcing the northward extension dynamically, addressed by Haarsma et al. (2008). Using a moisture tracer model, Bisselink and Dolman (2009) also found that advection is the most important contributor to precipitation over Central Europe. It is notable that the largest anomalies of T_{mean} and T_{max} responses to P_{JFM} (Fig. 1c, f) exist in Central Europe, while the largest T_{mean}

10 and T_{max} variance forced by P_{JFM} exists in Southeast Europe (Fig. 1a, d). This is because the interannual variability of T_{mean} as well as T_{max} over Central Europe is much stronger than that over Southeast Europe. We infer that the forced variance can be considered as the forcing strength or land-atmosphere coupling strength, while the forced anomalies cannot. It can also be noticed that the P_{JFM} variability forces large

15 T_{mean} and T_{max} variances over Southeast Europe (Fig. 1a, d), but that the variance of scPDSI is very limited there (Fig. 2a). This is possibly because the derived T_{mean} and T_{max} variability over Southeast Europe is closely related to the eastward extended heat response (Haarsma et al., 2008), while the soil moisture availability is very small there (Bisselink and Dolman, 2009).

20 We suggest that the NAO regime over the Mediterranean modulates summer climate over Europe through controlling winter precipitation that then initializes water cycle interactions with temperature. A positive phase of NAO tends to cause a hot and dry summer, or vice versa. This suggests there is scope for improved seasonal prediction of heat and drought waves from the pressure pattern of winter NAO. A remarkable

25 feature of the NAO is its prolonged positive phases in the past 40 years, possibly related to anthropogenic warming (Shindell et al., 1999). This NAO dry pattern over the Mediterranean may have contributed to the increased frequency of heat and drought waves since then through modulating the water interactions over the Mediterranean.

References

Alessandri, A. and Navarra, A.: On the coupling between vegetation and rainfall inter-annual anomalies: possible contributions to seasonal rainfall predictability over land areas, Geophys. Res. Lett., 35, L02718, doi:10.1029/2007GL032415, 2008.

Alfaro, E. J., Gershunov, A., and Cayan, D.: Prediction of summer maximum and minimum temperature over the Central and Western United States: the roles of soil moisture and sea surface temperature, J. Clim., 19, 1407–1421, 2006.

Bisselink, B. and Dolman, A. J.: Recycling of moisture in Europe: contribution of evaporation to variability in very wet and dry years, Hydrol. Earth Syst. Sci., 13, 1685–1697, doi:10.5194/hess-13-1685-2009, 2009.

Cassou, C., Terray, L., and Phillips, A. S.: Tropical Atlantic influence on European heat waves, J. Climate, 18, 2805–2811, 2005.

Cherchi, A., Gualdi, S., Behera, S., Luo, J. J., Masson, S., Yamagata, T., and Navarra, A.: The influence of tropical Indian Ocean SST on the Indian summer monsoon, J. Climate, 20, 3083–3105, 2005.

De Jeu, R. A. M., Wagner, W. W., Holmes, T. R. H., Dolman, A. J., van de Giesen, N. C., and Friesen, J.: Global soil moisture patterns observed by space borne microwave radiometers and scatterometers, Surv. Geophys., 29(4), 399–420, doi:10.1007/s10712-008-9044-0, 2008.

Della-Marta, P. M., Luterbacher, J. von Weissenfluh, H., Xoplaki, E., Brunnet, M., and Wanner, H.: Summer heat waves over Western Europe 1880–2003, their relationship to large-scale forcings and predictability, Clim. Dynam., 29, 251–275, 2007.

Ferranti, L. and Viterbo, P.: The European summer of 2003: sensitivity to soil water initial conditions, J. Climate, 19, 3659–3680, 2006.

Fischer, E. M., Seneviratne, S. I., Lüthi, D., and Schär, C.: Contribution of land-atmosphere coupling to recent European summer heat waves, Geophys. Res. Lett., 34, L06707, doi:10.1029/2006GL029068, 2007.

Haarsma, R. J., Selten, F., vd Hurk, B., Hazeleger, W., and Wang, X.: Drier Mediterranean soils due to greenhouse warming bring easterly winds over summertime Central Europe, Geophys. Res. Lett., 36, L04705, doi:10.1029/2008GL036617, 2009.

Hurrell, J. W., Kushnir, Y., and Visbeck, M.: The North Atlantic oscillation, Science, 291, 603–605, 2001.

Kettlewell, P. S., Stephenson, D. B., Atkinson, M. D., and Hollins, P. D.: Summer rainfall and wheat grain quality: relationships with the North Atlantic oscillation, Weather, 58, 155–164, 2003.

Meehl, G. A. and Tebaldi, C.: More intense, more frequent, and longer lasting heat waves in the 21st century, Science, 305, 994–997, 2004.

Mitchell, T. D. and Jones, P. D.: An improved method of constructing a database of monthly climate observations and associated high resolution grids, Int. J. Climatol., 25, 693–712, doi:10.1002/joc.1181, 2005.

Navarra, A. and Tribbia, J.: The coupled manifold, J. Atmos. Sci., 62, 310–330, 2005.

Pal, J. S., Giorgi, F., and Bi, X.: Consistency of recent European summer precipitation trends and extremes with future regional climate projections, Geophys. Res. Lett., 31, L13202, doi:10.1029/2004GL019836, 2005.

Qian, B. and Saunders, M. A.: Summer UK, Temperature and its links to preceding Eurasian snow cover, North Atlantic SSTs, and the NAO, J. Climate, 16, 4108–4120, 2003.

Richman, M. B. and Vermette, S. J.: The use of procrustes target analysis to discriminate dominant source regions of fine sulfur in the Western USA, Atmos. Environ., 27A, 475–481, 1993.

Seneviratne, S. I., Luethi, D., Litschi, M., and Schär, C.: Land-atmosphere coupling and climate change in Europe, Nature, 443, 205–209, 2006.

Seneviratne, S. I., Corti, T., Davin, E. L., Hirschi, M., Lehner, I., and Teuling, A. J.: Investigating soil moisture-climate interactions in a changing climate: a review, Earth-Sci. Rev., 99, 125–161, 2010.

Schär, C., Vidale, P. L., Lüthi, D., Frei, C., Häberli, C., Liniger, M. A., and Appenzeller, C.: The role of increasing temperature variability in European summer heatwaves, Nature, 427(322), 332–336, 2004.

European summer climate modulated by NAO-related precipitation

G. Wang et al.

Schär, C., Lüthi, D., and Beyerle, U.: The soil-precipitation feedback: a process study with a regional climate model, J. Climate, 12, 722–741, 1999.

Scherrer, S. C., Appenzeller, C., Liniger, M. A., and Schär, C.: European temperature distribution changes in observations and climate change scenarios, Geophys. Res. Lett., 32, L19705, doi:10.1029/2005GL024108, 2005.

Shindell, D. T., Miller, R. L., Schmidt, G., and Pandolfo, L.: Simulation of recent northern winter climate trends by greenhouse-gas forcing, Nature, 399, 452–455, 1999.

Stott, P. A., Stone, D. A., and Allen, M. R.: Human contribution to the European heatwave of 2003, Nature, 432, 610–614, 2004.

van der Schrier, G., Briffa, K. R., Jones, P. D., and Osborn T. J.: Summer moisture variability across Europe, J. Climate, 19, 2818–2834, 2006.

Vautard, R., Yiou, P., D'Andrea, F. de Noblet, N., Viovy, N., Cassou, C., Polcher, J., Ciais, P., Kageyama, M., and Fan, Y.: Summertime European heat and drought waves induced by wintertime Mediterranean rainfall deficit, Geophys. Res. Lett., 34, L07711, doi:10.1029/2006GL028001, 2007.

Wang, G., Dolman, A. J., Blender, R., and Fraedrich, K.: Fluctuation regimes of soil moisture in ERA40 re-analysis dataset, Theor. Appl. Climatol., 99, 1–8, 2010.

Wells, N., Goddard, S., and Hayes, M. J.: A self-calibrating Palmer drought severity index, J. Climate, 17, 2335–2351, 2004.

Zampieri, M., D'Andrea, F., Vautard, R., Ciais, P., de Noblet-Ducoudré, N., and Yiou, P.: Hot European summers and the role of soil moisture in the propagation of Mediterranean drought, J. Climate, 22, 4747–4758, 2009.

Zhang, J., Wang, W. C., and Leung, L. R.: Contribution of land-atmosphere coupling to summer climate variability over the contiguous United States, J. Geophys. Res., 113, D22109, doi:10.1029/2008JD010136, 2008.

Title Page

Abstract | Introduction

Conclusions | References

Tables | Figures

◄ | ►►

◄ | ►

Back | Close

Full Screen / Esc

Printer-friendly Version

Interactive Discussion

Table 1. A summery of the MCA analyses between P_{JFM} and the forced manifolds.

1st MCA mode	T_{mean}	T_{max}	scPDSI
explained squared covariance (%)	95	96	80
correlation coeficient	>0.99	>0.99	>0.99
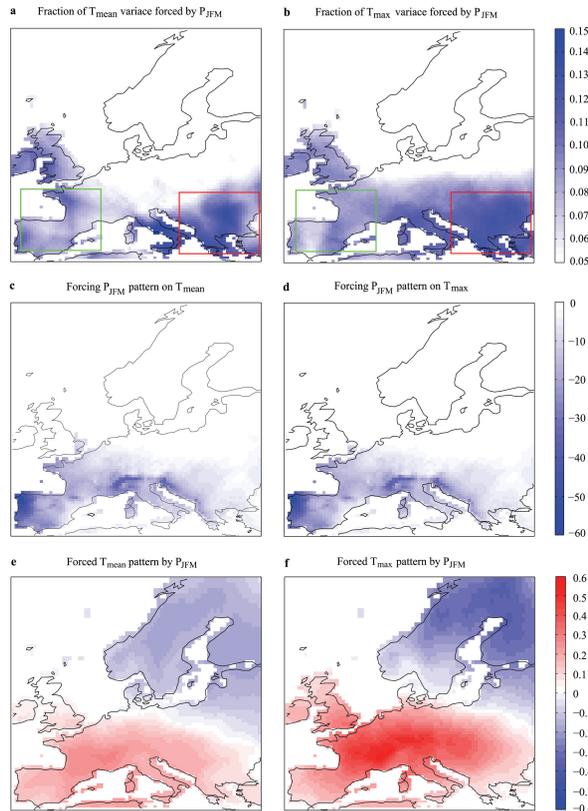
Fig. 1. T_{mean} as well as T_{max} variability forced by P_{JFM}. **(a)** Percentage of T_{mean} variance forced by P_{JFM} (sig=0.10 in the red rectangle). **(b)** The forcing P_{JFM} pattern and **(c)** its T_{mean} response. **(d)** Percentage of T_{max} variance forced by P_{JFM} (sig=0.10 in the red rectangle). **(e)** The forcing P_{JFM} pattern and **(f)** its T_{max} response. All the relevant time coefficient series mutually exhibit unit correlation ($r > 0.999$), shown in Fig. 3. Units are K for T_{mean} as well as T_{max} and mm for P_{JFM}.
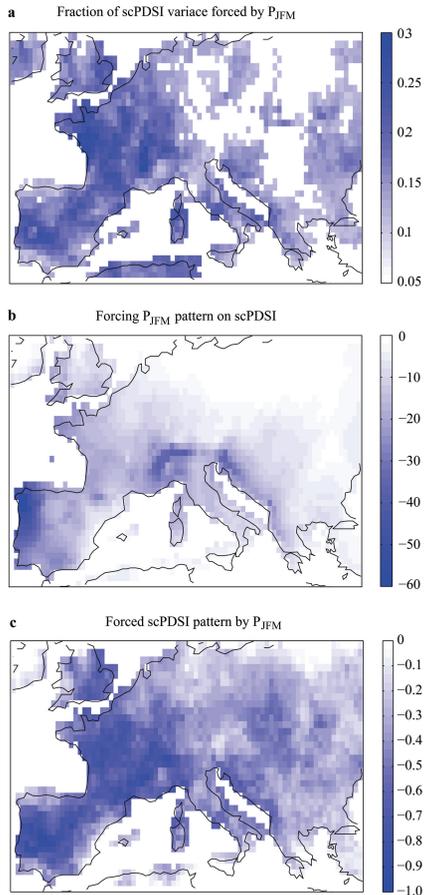
Fig. 2. The scPDSI variability forced by P_{JFM}. **(a)** Percentage of scPDSI variance forced by P_{JFM} (sig=0.01). **(b)** The forcing P_{JFM} pattern and **(c)** its scPDSI response, containing 80% of the total squared covariance. The MCA time coefficient series have unit correlation, shown in Fig. 3.
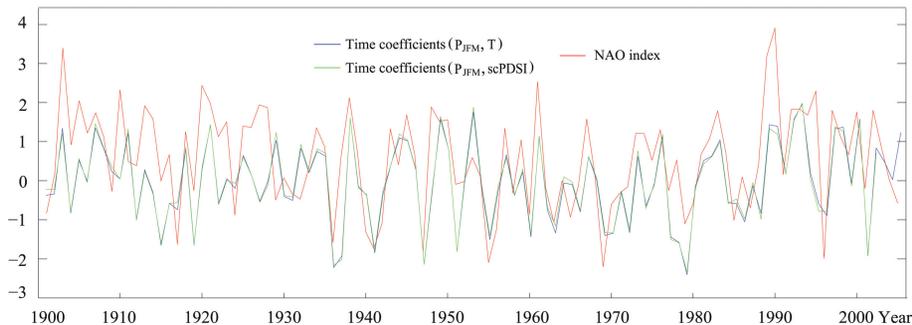
Fig. 3. The MCA time coefficient series and the NAO index. Green line indicates the time coefficients series for the MCA modes of P_{JFM} and T_{mean} as well as T_{max}. Four time coefficient series mutually have correlation $r > 0.999$, therefore shown with only on blue line. Green line indicates the unit correlated time coefficient series for the MCA mode of P_{JFM} and scPDSI. The red line indicates the averaged NAO index in January–March.